Early-life exposure to a potent Aryl hydrocarbon receptor ligand results in persistent changes to the microbiota and host glucose homeostasis

Yuan Tian
The Pennsylvania State University
Bipin Rimal
The Pennsylvania State University
Jordan E. Bisanz
The Pennsylvania State University
Wei Gui
Huck Institutes of the Life Sciences, The Pennsylvania State University
Trenton M. Wolfe
Montana State University
Imhoi Koo
The Pennsylvania State University
Iain M. Murray
The Pennsylvania State University
Shaneice K. Nettleford
The Pennsylvania State University
Shigetoshi Yokoyama
The Pennsylvania State University
Fangcong Dong
The Pennsylvania State University
K. Sandeep Prabhu
The Pennsylvania State University
Peter J. Turnbaugh
University of California San Francisco
Seth T. Walk
Montana State University
Gary H. Perdew
The Pennsylvania State University
Andrew D. Patterson (adp117@psu.edu)
The Pennsylvania State University

Research Article

Keywords: early-life exposure, persistent organic pollutants, 2,3,7,8-tetrachlorodibenzofuran, Akkermansia muciniphila, indole-3-lactic acid, glucose homeostasis

Posted Date: April 7th, 2023

DOI: https://doi.org/10.21203/rs.3.rs-2781053/v1

Abstract

Background Exposure to persistent organic pollutants (POPs) and gastrointestinal microbial disruption positively corelate with a predisposition to factors including obesity, metabolic syndrome, and type 2 diabetes; however, it is unclear if and how the microbiome contributes to this relationship.

Results Here, we show that early-life exposure to a potent aryl hydrocarbon receptor (AHR) agonist in mice resulted in persistent microbiota disruptions associated with impaired glucose homeostasis later in life. 2,3,7,8-tetrachlorodibenzofuran (TCDF)-exposed mice exhibited a profound disruption in the gut microbiome characterized by decreased abundances of *Akkermansia muciniphila* (*A. muciniphila*), decreased levels of cecal short chain fatty acids (SCFAs) and indole-3-lactic acid (ILA), and reduction of gut hormones GLP-1 and PYY. Importantly, microbial and metabolic phenotypes associated with early-life POP exposure were transferable to germ-free recipients in the absence of POP carry-over. Consistent with these in vivo studies, we reveal a direct, AHR-independent, POP-microbiota interaction that significantly affected the growth, physiology, gene expression, and metabolic activity of *A. muciniphila*, resulting in suppressed activity along the ILA pathway.

Conclusions These data point to a complex effect of POPs on the host and microbiota providing strong evidence that early-life, short-term, and self-limiting POP exposure can adversely impact the microbiome which persists into later life with associated health implications.

Background

Persistent organic pollutants (POPs) are a serious and global threat to human health due to their persistence, prevalence, and bio-accumulative nature. Exposure to POPs is associated with various health problems including cancer [1, 2], neurological disorders [3], immune suppression [4], reproductive disorders [5], and metabolic disease such as obesity [6, 7] and diabetes [8, 9]. Accumulating evidence suggests that exposure to POPs during early life may increase the risk of developing diabetes or obesity later in life in humans [10, 11]; however, the mechanisms of early-life exposure contributing to disease in adulthood remain poorly defined.

2,3,7,8-tetrachlorodibenzofuran (TCDF), a common environmental pollutant and POP, is a high affinity aryl hydrocarbon receptor (AHR) ligand. The AHR is the only ligand activated receptor in the Per-ARNT-Sim family of transcription factors that mediates the effects of a variety of exogenous and endogenous small molecules [12, 13]. In terms of structure and acute toxicity, TCDF is closely related to 2,3,7,8-tetrachlorodibenzo-*p*-dioxin (TCDD) whose toxicity is mediated solely through the AHR [14]. Unlike TCDD, TCDF has a short half-life (2–4 days in mouse and 1–3 years in human) and is quickly eliminated from the body relative to the more persistent TCDD (8–12 days in mouse and 7–10 years in human) [15, 16]. Previous studies revealed that five-day exposure to dietary TCDF rapidly altered the gut microbiota and disrupted host metabolism [17–19]. A recent study suggested that long-term exposure (continuous 14 weeks) to TCDF induced hepatic lipogenesis, an early hallmark of non-alcoholic fatty liver disease [20].

Although many studies report that POPs quickly and profoundly affect host health [18, 19], it is still unclear if and what are the long-lasting consequences after POPs (especially those with shorter half-lives) are eliminated from the body.

The gut microbiota plays major roles in maintenance of human health [21]. Gut microbial composition and functions are strongly influenced by diet, drugs, and environmental pollutants [22–24]. Importantly, growing evidence suggests that disrupted bacterial communities promoted by interventions such as antibiotic treatment early in life are associated with an increased risk of diseases in adulthood [25–27]. Our previous study reported that POPs not only altered bacterial physiology, but also significantly affected the metabolism of the microbial community, in addition to gene expression in vitro [28]. Recently, we also demonstrated that early-life exposure to 3,3',4,4',5-pentacholorobiphenyl (PCB 126), one of the most acutely toxic polychlorinated biphenyl (PCB) congeners with a long half-life, had a greater impact on bacteria in adulthood at the community structure, metabolic, and functional levels, independent of diet [29, 30]. These findings raise the possibility that microbial toxicity is a key target of early-life environment pollutant exposure that might be associated with increased risk of metabolic disorders later in life.

Here, we demonstrate that early-life exposure to TCDF, a representative of a large class of POPs including PCBs, dioxins, and dibenzofuran congeners that are AHR ligands [17–19], resulted in a profound disruption in the gut community structure and function that was associated with impaired glucose homeostasis later in life. Microbiota transplantation from TCDF-exposed mice into germ-free (GF) recipient mice resulted in reduction of cecal short chain fatty acids (SCFAs) and gut hormones glucagon-like peptide 1 (GLP-1) and peptide tyrosine-tyrosine (PYY). Consistent with the in vivo results, TCDF exposure not only affected the growth and physiology of *Akkermansia muciniphila* (*A. muciniphila*), but also altered its metabolism and gene expression including downregulation of the indole-3-lactic acid (ILA) pathway in vitro. This study provides new insights into the biochemical consequences of early-life environmental exposure involving the development of metabolic diseases later in life through the gut microbiota.

Results

Early-life TCDF exposure leads to persistent weight gain and glucose intolerance after TCDF is eliminated from the body

Given the considerably shorter half-life of TCDF in rodents relative to TCDD [15, 16], TCDF levels in the liver of mice from long duration (3 months after final exposure) were below the limit of detection via GC-MS (Fig. 1A-B). This observation was supported by data showing unchanged liver and ileal AHR target gene expression at three months after exposure compared with dramatically increased gene expression of those genes at short duration (the day after final exposure) (Fig. 1C-D). The significantly higher ratios of oxidized glutathione (GSSG) to reduced glutathione (GSH) and serum alkaline phosphatase (ALP) levels were observed with TCDF exposure at the short duration timepoint (Supplementary Figure S1A-B). No overt toxicity was observed at the long duration timepoint, supported by no significant changes in

serum ALP and cytokines, expression of intestinal cytokine mRNA, and liver histopathology (Supplementary Figure S1 and Supplementary Table S1). Interestingly, early-life five days of TCDF exposure significantly increased body weight and epididymal white adipose tissue (eWAT) later in life (Fig. 1E-F and Supplementary Figure S2). Impaired glucose tolerance was observed at three months after TCDF exposure (Fig. 1G), which was associated with significantly higher levels of liver glycogen and UDP-glucose (Fig. 1H). These data suggest that early-life TCDF exposure leads to higher body weight and glucose intolerance later in life after TCDF is eliminated from the body.

Early-life TCDF exposure rapidly increases liver lipogenesis in an AHR-dependent manner

Previous research has found that TCDF exposure induces hepatic lipid accumulation thus leading to nonalcoholic fatty liver disease[20, 31]. To investigate the effects of early-life TCDF exposure on liver lipid metabolism, we used ^{1}H NMR and mass spectrometry-based metabolomics along with conventional, GF and AHR knockout (*Ahr-/-*) mice. The triglyceride (TG) assay and quantitative ^{1}H NMR analysis showed significant increases in liver lipids with TCDF exposure at the short duration timepoint (Fig. 2A-B). UHPLC-MS/MS global analysis also confirmed that five days of TCDF exposure immediately resulted in dramatic changes in liver lipid (Fig. 2C and Supplementary Table S2). Subtle changes in liver profiles were observed with TCDF exposure at three months after exposure (Fig. 2A-C and Supplementary Table S2), which was consistent with no obvious changes in hepatic fat accumulation (Oil Red O staining) or macrophages (F4/80-positive cells) from TCDF-exposed mice from the long duration timepoint (Supplementary Figure S3). To further explore the effect on lipid metabolism, fatty acid compositional analysis was performed using ^{1}H NMR and GC-MS. Consistently, quantitative ^{1}H NMR and targeted GC-MS analysis revealed significantly higher levels of hepatic fatty acids from TCDF-exposed mice at the short duration timepoint (Fig. 2D and Supplementary Figure S4). TCDF did not result in dramatic changes in fatty acid profiling in liver at three months after exposure (Fig. 2D and Supplementary Figure S4). Consistent with the metabolomics data, mRNA expression of genes involved in *de novo* fatty acid biosynthesis was also significantly higher in the liver at the short duration timepoint but few changes at the long duration timepoint after TCDF exposure (Fig. 2E).

To test whether these lipid changes by TCDF exposure could be specific to AHR activation or microbiota changes, we measured the liver lipid profile in *Ahr-/-* and GF mice with five days of TCDF exposure (Fig. 2F-H and Supplementary Figures S5). No significant changes in the lipid profile or mRNA expression of liver AHR target genes were observed in *Ahr-/-* mice with five days of TCDF exposure (Fig. 2F-H). However, we observed significantly higher levels of liver lipids as well as induction of mRNA expression of AHR target genes in GF mice with five days of TCDF exposure (Supplementary Figure S5). Together, these data suggest that TCDF exposure rapidly increases liver lipogenesis that is specific to AHR activation but not due to microbiota changes.

Early-life TCDF exposure impacts the gut microbiome composition and function later in life

Recent evidence demonstrated that dietary TCDF rapidly induced a remarkable change in the overall population of gut microbiota [19]. To further explore the long-term influence of early-life TCDF exposure on the gut microbiota, metagenomics and metabolomics analysis were performed. Principal coordinate analysis of cecal species-level abundances revealed significant effects of TCDF exposure on the microbiome composition only later in life (Fig. 3A). Five days of TCDF exposure resulted in significant decreases in relative abundances of species *Akkermansia muciniphila*, *Parasutterella excrementihominis*, and *Bifidobacterium pseudolongum* and an increase in relative abundance of species *Methanomethylovorans SGB40959* at three months after exposure (Fig. 3B and Supplementary Table S3). Analysis of differentially abundant gene families identified genes corresponding to amino acid, nucleotide, and carbohydrate metabolism that were significantly regulated by TCDF exposure later in life (Fig. 3C and Supplementary Table S4).

We then sought to investigate the influence of early-life TCDF exposure on microbial function (Fig. 3D-F). Significant changes in urinary bacterial metabolites and circulating lipopolysaccharide (LPS), the primary component of the outer membrane of Gram-negative bacteria [17], were observed with TCDF exposure later in life (Supplementary Figure S6). The significant lower levels of cecal tryptophan metabolite indole-3-lactic acid (ILA) that is associated with intestinal inflammation [32] were observed with TCDF exposure later in life (Fig. 3D and Supplementary Table S5). TCDF exposure also resulted in the significantly lower levels of short-chain fatty acids (SCFAs) later in life, which was confirmed with the significantly lower mRNA expression for G protein-coupled receptors (GPCRs) including GPR41, GPR43, and GPR119 in colon tissues (Fig. 3F), receptors activated by SCFAs [33, 34]. The mRNA expression for GLP1 and PYY also showed significantly lower levels in colon tissues from mice with TCDF exposure later in life (Fig. 3F).

Next, we investigated whether this effect could be transferred to GF mice via cecal microbiota transplantation (Fig. 3G-J and Supplementary Figure S7). Two weeks after conventionalization with either cecal contents from control mice or those treated with TCDF, mice exhibited a stable gut microbiome but no changes in the body weight gain (Supplementary Figure S7A-B). GF recipients from TCDF exposed mice exhibited significantly lower levels of cecal SCFAs and mRNA expression of GPCRs and gut hormones GLP1 and PYY in the colon after 4 weeks conventionalization (Fig. 3G-H). Moreover, we observed significantly higher levels of liver UDP-glucose as well as mildly increased liver glucose (P = 0.06) and fasting blood glucose levels (P = 0.06) in GF recipients from TCDF exposed mice after 4 weeks conventionalization (Fig. 3I-J). No significant changes in expression of liver AHR target gene or lipid profiling were observed in TCDF-transplantation mice after 4 weeks conventionalization (Supplementary Figure S7C-E). These results suggest that early-life TCDF exposure impacts the gut microbiome composition and function later in life in the absence of POP carry-over.

A. muciniphila is negatively correlated with TCDF exposure and its administration promotes production of indole-3-lactic acid and short chain fatty acids

As one of promising probiotics, *A. muciniphila*, as a key mucin-degrading bacterium [35], has been proven to be closely related to the metabolic diseases of its human host [36, 37]. Our findings revealed that early-life TCDF exposure resulted in significantly lower abundances of cecal *A. muciniphila* at three months after exposure (Fig. 4A-B), which was consistent with the significantly higher levels of fecal mucin (Supplementary Figure S8). GF recipients from TCDF exposed mice also exhibited significantly lower abundances of cecal *A. muciniphila* (Fig. 4C).

Next, to directly examine the functional role of *A. muciniphila* that is negatively correlated with TCDF exposure in vivo, we colonized antibiotic-treated or non-treated GF mice with *A. muciniphila* (Fig. 4D-H). Interestingly, colonized with *A. muciniphila* activated AHR target gene expression in colon (Fig. 4E) but remained unchanged in the liver and ileum (Supplementary Figure S9), consistent with significant higher levels of cecal tryptophan metabolites including ILA, considered to be reliable sources of AHR ligands [13] (Fig. 4F and Supplementary Table S6). Furthermore, GF mice colonized with *A. muciniphila* exhibited significantly higher levels of cecal SCFAs and mRNA expression of GPCRs and gut hormones in the colon (Fig. 4G-H). These data demonstrate a direct contribution of *A. muciniphila* in the production of healthy promoting microbial metabolites in the intestine that is negatively correlated with TCDF exposure.

TCDF exposure significantly affect the metabolism of A. muciniphila **in vitro**

Next, we focused on the effect of TCDF on *A. muciniphila* in vitro. Consistent with the in vivo study, the significant decreases in the growth of *A. muciniphila* were observed with two doses of TCDF (0.6 μM and 6 μM) exposure in vitro (Fig. 5A). The high dose of TCDF (6 μM) significantly increased the proportions of damaged bacteria (Pi-stained) and decreased CFDA-stained cells (Fig. 5B). No significant effects were observed in the proportions of SybrGreen and $DiBAC_4$-stained bacteria with the two doses of TCDF exposure (Supplementary Figure S10).

To further explore the influence of TCDF on *A. muciniphila*, transcriptomics (RNA-Seq) coupled with metabolomic analysis were performed (Fig. 5C-H). PCA analysis of the RNA-seq data showed distinct separation between *A. muciniphila* with vehicle and two doses of TCDF (0.6 μM and 6 μM) (Fig. 5C). Among the 615 significantly changed genes, 35 genes were downregulated and 12 genes were upregulated with fold changes > 1.5 in *A. muciniphila* with higher dose of TCDF (6 μM) compared to vehicle (Fig. 5D). Gene orthologs involved in amino acid metabolism, carbohydrate metabolism, nucleotide metabolism, membrane integration, vitamin metabolism, and translation pathways were most significantly reduced in *A. muciniphila* with two doses of TCDF exposure (0.6 μM and 6 μM) (Fig. 5E and Supplementary Table S7). Of particular note, the significant downregulation of *A. muciniphila*-derived ILA pathway was observed with higher dose of TCDF (6 μM) compared to vehicle (Fig. 5F and Supplementary Tables S7-8). UHPLC-MS-based global metabolomic analysis revealed the marked decrease in carbohydrate, amino acid, and nucleotide metabolism by two doses of TCDF exposure (Fig. 5G and Supplementary Table S9). Moreover, significant increases in bacterial membrane lipids including carnitine

(CAR), ceramide (Cer), sphingolipid (SL), lysophosphatidylcholine (LPC), sphingomyelin (SM), diglycerol (DG), and TG were observed in two doses of TCDF exposure (Fig. 5H and Supplementary Table S10), in agreement with our previous result showing profound changes in bacterial lipid profiles following four POPs exposure in vitro [28].

Discussion

This study is, to our knowledge, the first example suggesting that early-life disruptions in the gut microbiome by environmental pollutants are important mechanisms linking the association between environmental pollutant exposure and metabolic disorders later in life. Infants and children may have increased exposure to environmental chemicals compared to adults or may have been exposed in utero and via breast milk [38–41], but only limited attention has been given to the subsequent outcomes [42]. Our work demonstrates that early-life exposure to an environmental pollutant increases the risk of metabolic disorders later in life by a prominent disruption in the gut microbiome.

Establishment of the microbiome in early life is gaining appreciation as a major influencer in human development and long-term health outcomes [43, 44]. Accumulating evidence suggests that microbiota disruptions by antibiotic exposure in early life can have long-lasting effects on host health and significantly increase the risk of developing obesity and associated metabolic disorders later in life [27, 45]. Currently, POPs are increasingly recognized as influential modulators of the gut microbiota [17, 19, 28]. We observed a long-lasting impact on the gut microbiota by early-life TCDF exposure. For example, early-life TCDF exposure resulted in the significant decreases in species *A. muciniphila* and *Bifidobacterium pseudolongum* later in life, which may confer a significant health benefit to the host [35, 36, 46]. The increased levels of circulating LPS and decreased levels of cecal ILA later in life were observed with early-life TCDF exposure, suggesting the intestinal inflammation and immune dysregulation [6, 17].

Our data indicate that disruption of the gut microbiome by early-life TCDF exposure is associated with impaired glucose homeostasis later in life. Altered gut microbiota composition and function have been associated with obesity and obesity-related metabolic disorders in animals and humans [47, 48]. Recent in vivo and in vitro studies suggest that SCFAs, the primary metabolites of gut microbiota, may regulate host energy metabolism by increasing gut hormones such as PYY and GLP-1 via activation of SCFA receptors [49, 50]. Changes in the microbiome community, decreases in colonic SCFAs levels, inhibition of GLP-1 signaling, and reduced insulin sensitivity have been reported by antibiotic treatment [51]. Similarly, we also observed decreased levels of cecal SCFAs as well as lower expression of SCFA receptors and gut hormones GLP-1 and PYY later in life with early-life TCDF exposure, which likely contribute to impaired glucose homeostasis and development of obesity [52]. Remarkably, we observe that this effect could be transferred to GF mouse recipients with microbiota transplantation from TCDF-exposed mice. Our study supplies evidence in a mouse model linking disturbances in the gut microbiota with early-life

environmental pollutant exposure and the subsequent development of metabolic diseases. This study helps to illustrate the importance of the microbiome as a key target of early-life environmental pollutant exposure. TCDF is one model for the presence of a variety of AHR persistent ligands and looking at risk of early-life exposure needs to take into account all of these compounds in future studies.

There is increasing discussion regarding *A. muciniphila* as a beneficial player in the maintenance of gut health and host glucose homoestasis [35–37]. Supplementation with *A. muciniphila* in overweight and obese humans improves several metabolic parameters in clinical trials [37, 53]. In this work, we observed significantly reduced levels of *A. muciniphila* by TCDF exposure in both in vivo and in vitro models. Consistently, the reductions in carbohydrate metabolism, amino acid metabolism, and nucleotide metabolism were also observed in *A. muciniphila* with TCDF exposure at the transcriptional and metabolic levels in vitro. The profound changes in the lipid profile of *A. muciniphila* by TCDF exposure were observed, which indicated disturbances in bacterial membrane function [28]. Specifically, TCDF exposure significantly downregulated *A. muciniphila*-derived ILA pathway in vitro, which is consistent with in vivo showing significant lower levels of cecal ILA with early-life TCDF exposure. The presence of ILA has recently been reported in breastfed infants colonized with *Bifidobacterium infantis*, and this microbial tryptophan metabolite has been shown to decrease enteric inflammation through activation of AHR [32, 54]. However, relatively little is known about which and how the other microbiota regulate this anti-inflammatory metabolite. We have demonstrated that *A. muciniphila* has capable of producing ILA, which is negatively correlated with TCDF exposure in both in vitro and in vivo. A more comprehensive understanding of the dynamics of microbial tryptophan catabolites and their functional implication during early life environmental exposure is needed. Our data described here suggests that the significant impact of TCDF exposure to *A. muciniphila* could be a contributing factor that mediates the relationship between early-life TCDF exposure and the potential increased risk of metabolic disorder later in life.

Conclusions

Our work demonstrates that early-life exposure of TCDF resulted in a persistent and profound disruption in gut microbiome that was associated with the development of obesity and impaired glucose homeostasis later in life. We find TCDF exposure reduced a beneficial microbe, *A. muciniphila*, and that reduction was observed in in vivo and in vitro models. This study provides new insight into microbiota-derived cues that drive the development of metabolic diseases later in life.

Materials And Methods

Chemicals

Sodium 3-(trimethylsilyl) [2,2,3,3-$^{2}H_4$] propionate (TSP), D_2O (99.9% in D), and TCDF were obtained from Cambridge Isotope Laboratories, Inc. (Tewksbury, MA). Transgenic dough pills were obtained from Bio-Serve (Flemington, NJ). Fatty acid standards, tryptophan metabolites, and their deuterated internal standards were purchased from Sigma-Aldrich (St Louis, MO) and Cayman Chemical (Ann Arbor, MI).

In vitro bacterial culture and flow cytometry

A. muciniphila DSM 22959 was cultured using BHI CHV media (for more detailed methods about media preparation, see Supplemental Material) and treated with two doses of TCDF (high: 6 μM and low: 0.6 μM) at 37°C for 72 h. The growth rate of *A. muciniphila* was measured by optical density (OD 600) using a Multiskan Sky Microplate spectrophotometer (Thermo Fisher Scientific, Waltham, MA). Flow cytometry, metabolomics, and transcriptomics analysis were performed after 36 h of incubation. The in vitro experiment was performed in a monitored anaerobic chamber (Coy Laboratory Products, 95% N_2, 5% H_2) and repeated at least three times.

After incubation, *A. muciniphila* was washed and resuspended with 1X reduced PBS containing 1 mg/mL L-cysteine. Bacteria samples were stained by four fluorescent dyes for physiology assessing including SybrGreen, Pi, CFDA, and $DiBAC_4$ [28, 55]. All cytometric analyses were analyzed on a BD Accuri™ C6 plus flow cytometer (BD Biosciences, San Jose, CA), and data were analyzed with FlowJo V10 software (FlowJo, LLC, Ashland, OR). The percentages of Pi, CFDA, and $DiBAC_4$ stained cells were normalized to the total bacterial counts obtained by SybrGreen staining.

Mice

Male C57BL/6J wild type mice were used in the four series of experiments. A complete description of the mouse experiments is provided in supplemental materials. The experiments were performed using protocols approved by the Pennsylvania State University (PROTO202001416) and Montana State University (2022-54-117) Institutional Animal Care and Use Committee. A subset of 3-week-old male C57BL/6J mice were fed pills containing TCDF (a final dose of 24 μg/kg) or control for 5 days. Two models were used to evaluate the effect of early-life TCDF exposure on mice (Fig. 1A). Mice were sacrificed on the day after the last TCDF exposure (short-term model) or sacrificed at 3 months after POP exposure (long-term model). TCDF (24 μg/kg) or corn oil as vehicle were administered to male GF and *Ahr-/-* mice by oral gavage once daily for five days. Cecal microbiota transplantation was performed as following (Fig. 3G): GF mice were orally gavaged with 100 μL of cecal suspension (100 mg in 1 mL sterile BHI CHV media) from vehicle or TCDF treated mice in long-term model. After week four post-transplantation, mice were fasted for 6h and measured glucose levels prior to sacrifice. For *A. muciniphila* colonization experiments following antibiotic treatment (Fig. 4D), mice were orally gavaged with *A. muciniphila* at one dose of 10^7 CFU/0.1 mL, followed by 2 weeks of antibiotic cocktail solution composed of 2 mg/mL neomycin, 2 mg/mL streptomycin and 2 mg/mL bacitracin in drinking water. Control groups were administered 2 weeks of antibiotic cocktail solution without *A. muciniphila* colonization.

Histopathology And Immunohistopathology

Formalin-fixed liver tissues were embedded in paraffin wax, sectioned (3–5 μm), and stained with hematoxylin and eosin (H&E). Liver oil red O staining was performed on optimal cutting temperature (OCT)-embedded frozen liver sections by Histoserv, Inc (Germantown, MD). Frozen liver sections were stained with rat monoclonal anti-mouse macrophage F4/80 (1:100, Invitrogen, Carlsbad, CA), followed by an incubation of anti-mouse IgG HRP-conjugated antibody (1:200, Invitrogen, Carlsbad, CA), according to "Immunohistochemistry Protocol for Frozen Sections" (BioLegend, San Diego, CA).

Blood clinical biochemistry and cytokine analysis

Serum alkaline phosphatase (ALP) was measured using the VetScan VS2 and the Mammalian Liver Profile rotor (Abaxis Inc., Union City, CA) according to the manufacturer's instructions. Serum cytokine levels were measured with a BioPlex 200 mouse cytokine array/ chemokine array 32-Plex by Eve Technologies (Calgary, Canada).

Liver Triglyceride And Glutathione Quantification

Liver triglyceride (TG) was measured using Triglyceride Colorimetric Assay Kit according to the manufacturer's protocol (Cayman Chemical, Ann Arbor, MI). The ratios of reduced glutathione (GSH) and oxidized glutathione (GSSG) were measured with GSH/GSSG Ratio Detection Assay Kit according to the manufacturer's recommendation (Abcam, Cambridge, United Kingdom).

Fecal Mucin And Serum Lipopolysaccharide Quantification

Fecal mucin levels were measured using Fecal Mucin Assay Kit according to the manufacturer's protocol (Cosmo Bio USA, Carlsbad, CA). Serum LPS levels were measured using Pierce™ LAL Chromogenic Endotoxin Quantitation Kit (Thermo Fisher Scientific, Waltham, MA).

Glucose Tolerance Test

Glucose tolerance test was done as previously described [56] and followed a 6h fast. In brief, blood glucose was measured following intraperitoneal injection of 40% glucose (2.0 g/kg body weight). The blood glucose concentrations were measured using OneTouch Ultra 2 Meter (LifeScan, Malvern, PA).

Quantification Of Tcdf In Liver Tissues

Liver (500 mg) was extracted with 10 mL of 6M hydrochloric acid and 10 mL of chloroform/hexane mix [1:1 (v/v)]. After centrifugation, the top layer was dried in a vacuum and reconstituted in 2 mL of hexane, followed by cleaning using a florisil column as per USEPA-1613. Column packing materials for the cleanup procedure included anhydrous sodium sulfate and Florisil 60–100 mesh from Restek (Bellefonte, PA). Liver TCDF levels was measured by an Agilent 7890A-5975C GC-MS system (Agilent Technologies,

Santa Clara, CA) equipped with a Rxi-5ms (Restek) capillary column (30 m, 0.25 mm ID, 0.25 μm film thickness). The results were quantified by a standard curve. The limit of detection is 10 pg/L.

Tissue Rna Isolation And Qpcr

RNA was extracted from liver and intestine tissues using TRIzol reagent (Invitrogen, Carlsbad, CA) according to the manufacturer's instruction. The cDNA was synthesized from 1 μg of RNA using qScript cDNA SuperMix (Quanta Biosciences, Gaithersburg, MD). Quantitative PCR (qPCR) reactions were carried out using PowerUp SYBR Green Master Mix (Applied Biosystems, Waltham, MA) with a QuantStudio 3 real-time PCR system (Thermo Fisher Scientific, Waltham, MA). The primers can be found in Supplementary Table S11. The data were analyzed according to the ΔΔCT method.

^{1} H NMR based metabolomics experiments

Hydrophilic metabolites from cecal content, liver, and urine samples for NMR analysis were extracted as previously described [57]. Liver lipid quantification was done using published methods [58], with minor modifications. Briefly, 50 mg of liver tissue was homogenized in 1 mL pre-cooled chloroform/methanol mix [1:1 (v/v)], followed by adding 296 μL water. After centrifugation, the lower phase was dried in a vacuum and reconstituted in 600 μL of deuterated chloroform containing 0.03% (v/v) tetramethylsilane (TMS). ^{1}H NMR spectra were acquired using a Bruker Avance NEO 600 MHz spectrometer equipped with an inverse cryogenic probe (Bruker Biospin, Germany) at 298 K. NMR spectra of the liver, cecal content, and urine samples were recorded with a typical 1D NMR spectrum named NOESYPR1D. The metabolites were assigned on the basis of a set of 2D NMR spectra and published results [58, 59]. All ^{1}H NMR spectra were corrected for phase and baseline distortions and quantified for hydrophilic metabolites using Chenomx NMR Suite 8.4 (Chenomx Inc., Edmonton, AB, Canada). The absolute quantification for lipid classed in liver were calculated as previously reported [18, 58].

Tryptophan Metabolites Quantitation By Uhplc-ms/ms

Target analysis of tryptophan metabolites in mouse cecal content and *A. muciniphila* was performed using a reverse-phase UHPLC Prominence 20 UFLCXR system coupled to a 5600 (QTOF) TripleTOF using a Duospray™ ion source (AB Sciex, Framingham, MA, USA) with a Waters BEH C18 (2.1 × 100 mm, 1.7 μm particle size) UPLC column [60]. Mouse cecal contents (10 mg) or *A. muciniphila* (1.5 mL) were extracted with 100 μL ice-cold 10% acetonitrile (v/v) containing 1 μM deuterated internal standards. Following homogenization and centrifugation, 50 μL of the supernatant was transferred to an autosampler vial. The results were quantified by comparing integrated peaks against a standard curve.

LC-MS based metabolomics experiments

Lipid analysis of liver and bacteria samples was performed using a Vanquish UHPLC system (Thermo Fisher Scientific, Waltham, MA) connected to an Orbitrap Fusion Lumos Tribrid™ mass spectrometer

using a H-ESI™ ion source (all Thermo Fisher Scientific) with a Waters (Milford, MA) CSH C18 column (1.0 × 150 mm, 1.7 µm particle size). Hydrophilic metabolites of mouse cecal and bacteria were performed with a Dionex Ultimate 3000 quaternary HPLC system connected to Exactive™ Plus Orbitrap mass spectrometer (Thermo Fisher Scientific, Waltham, MA) with a Waters XSelect HSS T3 column (2.1 × 100 mm, 2.5 µm particle size).

The liver samples (20 mg) were extracted twice with 0.5 mL of pre-cool isopropanol/water/ethyl acetate (30:10:60, v/v/v) containing 1:1000 EquiSPLASH (Avanti Polar Lipid, Alabaster, AL). After homogenization and centrifugation, the combined supernatants were dried in a vacuum and reconstituted in 200 µL of isopropanol/acetonitrile/H_2O (45:35:20, v/v/v). After a centrifugation, 40 µL of supernatants were transferred to autosampler vials for LC-MS analysis. The hydrophilic metabolites and lipid of bacteria were extracted as previously described [28]. LC-MS data were analyzed by the open-source software MS-DIAL [61]. MetaMapp network analysis for bacteria hydrophilic metabolites was performed to visualize and integrate biochemical pathways and chemical similarities [55, 62]. Heatmaps were plotted using R software package “pheatmap”.

Fatty acid analysis by GC–MS

Quantitative measurements of liver fatty acids were performed as previously reported [63, 64]. Briefly, liver (10 mg) samples were homogenized in 500 µL of methanol containing fatty acid internal standards. After acetyl chloride catalyzed methyl esterification, the identification and quantification of methylated fatty acids was performed on an Agilent 7890A-5975C GC-MS system (Agilent Technologies, Santa Clara, CA) equipped with a Rxi-5ms (Restek) capillary column (30 m, 0.25 mm ID, 0.25 µm film thickness). The amounts of fatty acids were determined relative to internal standards.

Bacteria DNA isolation and qPCR

The DNA of *A. muciniphila* and mouse intestinal content samples was extracted using E.Z.N.A. stool DNA kit (Omega Bio-Tek Inc., Norcross, GA) according to the manufacture's protocol. Total bacteria and *A. muciniphila* quantification were calculated using a standard curve with the threshold (C_T) value versus the number of bacterial CFUs [65]. qPCR reactions were carried out with PowerUp SYBR Green Master Mix (Applied Biosystems, Waltham, MA) on a QuantStudio 3 real-time PCR system (Thermo Fisher Scientific, Waltham, MA). Primers can be found in Supplementary Table S12. Reactions were performed using the cycle conditions (50°C, 2 min, 95°C, 2 min; 95°C, 1 s, 60°C, 30 s, for 45 cycles; 95°C, 15 s, 60°C, 1 min, 95°C, 15 s).

Metagenomic Analysis

Mouse cecal DNA samples were sequenced using NextSeq Mid-Output 150 x 150 paired end sequencing. The resulting reads were processed using fastp v 0.23.2 [66] with automatic adapter detection, poly G removal, and sliding window quality filtering. After QC, the median sequencing depth was 2.69 Gb (range

2.08–3.8). To obtain highest possible assignment rates of mice taxa, taxonomic characterization was performed with MetaPhlAn4 version 4.0.6 [67] which incorporating species-level genome bins (10.1016/j.cell.2019.01.001) with additional estimation of the unassigned fraction. The median unassigned percentage was 20.03 (range 9.30–59.33); however, this did not vary significantly between treatment groups ($P > 0.05$, Mann-Whitney U test). To negate any potential effects of variable unassigned taxa, data were transformed by centered log ratio with zeros replaced with 2/3s of the lowest detected relative abundance on a per sample basis, and ordinations performed using the Aitchison / CLR Euclidean distance (10.3389/fmicb.2017.02224). Statistical analysis of distance matrices was performed using ADONIS2/permanova function of vegan 2.6-4 [68]. Statistical analysis of differential species abundance was performed using a Mann-Whitney U test followed by a Benjamini Hochberg False Discovery rate correction with significance determined as FDR < 0.2. Gene family abundances were calculated using HUMAnN v3.5 against the UniRef90 Metacyc 25 databases [69]. Gene family abundances were normalized to RPKG (reads per thousand bases per genome equivalent) by estimating genome equivalents using MicrobeCensus (10.1186/s13059-015-0611-7). Statistical testing of gene family abundances was performed using Welch's t-test with a Benjamini Hochberg False Discovery Rate cutoff of 0.2.

Transcriptomic Analysis

Total RNA was isolated from 7 mL of *A. muciniphila* culture by addition of 1 mL of Trizol and the DNA was removed by RNase-Free DNase Set (QIAGEN, Hilden, Germany). After purification with PureLink™ RNA Mini Kit (Invitrogen, Carlsbad, CA), total RNA was measured and checked by an Agilent Bioanalyzer. The 16S and 23S rRNA fractions were removed from total RNA using the RiboMinus™ Bacteria 2.0 Transcriptome Isolation kit (Invitrogen, Carlsbad, CA). The deletion of 16S and 23S rRNA was checked again with the Agilent Bioanalyzer. Depleted RNA samples were submitted to Microbial Genome Sequencing Center (Pittsburgh, PA) for RNA sequencing. Library prep was performed using Illumina Stranded RNA library kit and sequenced on a MiSeq to generate about 12 million 50bp paired end reads per sample.

Obtained demultiplexed reads were checked for quality using Fastp [66] to remove bad quality reads, low complexity regions and adapters. Kraken2 was used to check for contamination of reads by other bacteria [70]. Filtered reads were then aligned to *A. muciniphila* ATCC BAA-835 reference assembly (GCF_000020225.1_ASM2022v1) using bowtie2 [71]. Alignment qualities were checked using Qualimap [72]. featureCounts function of Rsubread package in R was used to count the reads in terms of coding sequences (CDS) [73]. Only uniquely mapped reads were considered for counting. Raw counts were then normalized and then analyzed for differential gene expression using DESeq2 package [74]. Further, visualization and analysis were performed in R and GraphPad Prism 6.0 (GraphPad, San Diego, CA).

Transcriptomic And Metabolomics Data Integration And Visualization

Metabolomics data and transcriptomics data were visualized using MetaboMAPS [75]. Pathway was condensed into a custom figure. The enzymes were mapped to genes. The concentration of metabolites and Log2Fold changes in genes were plotted on the graph as bar and circle.

Sanger Sequencing

The DNA from *A. muciniphila* was confirmed by Sanger sequencing as previously described [55]. The result was analyzed with BLAST (Supplementary Table S13).

Statistics

All data values are expressed as mean ± standard deviation (SD) or median and interquartile ranges. Graphical illustrations and statistical analyses were performed using GraphPad Prism 6.0 (GraphPad, San Diego, CA). Two-tailed unpaired t test analyses or Mann-Whitney U test in vivo study and one-way analysis of variance (ANOVA) followed by Dunnett's multiple comparisons in vitro study were used. Adjusted *P* values were calculated using Tukey's correction.

Declarations

Acknowledgements

Not applicable.

Author Contributions

Y.T. G.H.P, and A.D.P. conceived the project. Y.T., B. R., W. G., J. E. B., T. M. W., S. K. N., S. Y., and F. D. performed experiments and analyzed data. Y. T., B. R., J. E. B., and S. K. N. performed bioinformatics analysis and results interpretation. Y.T. and A.D.P. wrote the manuscript. All authors edited and approved the final manuscript.

Funding

ADP was supported by NIH grants (ES028288, S10OD021750), the PA Department of Health using Tobacco CURE funds, and the USDA National Institute of Food and Federal Appropriations under Project PEN047702 and Accession number 1009993. GHP was supported by NIH grant R35 ES028244.

Availability of data and materials

The data that support the findings of this study are available from the corresponding author upon request. The raw sequences have been deposited in the National Center for Biotechnology Information (NCBI) database with accession number PRJNA952227 for metagenomics sequences and transcriptomics sequencing.

Ethics approval and consent to participate

Not applicable.

Consent for publication

Not applicable.

Competing interests

The authors declare that they have no competing interests.

References

1. Koual M, Cano-Sancho G, Bats AS, Tomkiewicz C, Kaddouch-Amar Y, Douay-Hauser N, Ngo C, Bonsang H, Delomenie M, Lecuru F, et al: Associations between persistent organic pollutants and risk of breast cancer metastasis. Environ Int 2019, 132:105028.
2. Wielsoe M, Kern P, Bonefeld-Jorgensen EC: Serum levels of environmental pollutants is a risk factor for breast cancer in Inuit: a case control study. Environ Health 2017, 16:56.
3. Grova N, Schroeder H, Olivier JL, Turner JD: Epigenetic and Neurological Impairments Associated with Early Life Exposure to Persistent Organic Pollutants. Int J Genomics 2019, 2019:2085496.
4. Gascon M, Morales E, Sunyer J, Vrijheid M: Effects of persistent organic pollutants on the developing respiratory and immune systems: A systematic review. Environ Int 2013, 52:51–65.
5. Vested A, Giwercman A, Bonde JP, Toft G: Persistent organic pollutants and male reproductive health. Asian J Androl 2014, 16:71–80.
6. Lee DH, Porta M, Jacobs DR, Vandenberg LN: Chlorinated Persistent Organic Pollutants, Obesity, and Type 2 Diabetes. Endocr Rev 2014, 35:557–601.
7. Dirinck E, Jorens PG, Covaci A, Geens T, Roosens L, Neels H, Mertens I, Van Gaal L: Obesity and Persistent Organic Pollutants: Possible Obesogenic Effect of Organochlorine Pesticides and Polychlorinated Biphenyls. Obesity 2011, 19:709–714.
8. Magliano DJ, Loh VHY, Harding JL, Botton J, Shaw JE: Persistent organic pollutants and diabetes: A review of the epidemiological evidence. Diabetes Metab 2014, 40:1–14.
9. Lee YM, Jacobs DR, Lee DH: Persistent Organic Pollutants and Type 2 Diabetes: A Critical Review of Review Articles. Front Endocrinol 2018, 9:712.
10. Karlsen M, Grandjean P, Weihe P, Steuerwald U, Oulhote Y, Valvi D: Early-life exposures to persistent organic pollutants in relation to overweight in preschool children. Reprod Toxicol 2017, 68:145–153.
11. Tang-Peronard JL, Jensen TK, Andersen HR, Ried-Larsen M, Grontved A, Andersen LB, Timmermann CAG, Nielsen F, Heitmann BL: Associations between Exposure to Persistent Organic Pollutants in Childhood and Overweight up to 12 Years Later in a Low Exposed Danish Population. Obes Facts 2015, 8:282–292.

12. Beischlag TV, Morales JL, Hollingshead BD, Perdew GH: The aryl hydrocarbon receptor complex and the control of gene expression. Crit Rev Eukaryot Gene Expr 2008, 18:207–250.
13. Hubbard TD, Murray IA, Perdew GH: Indole and Tryptophan Metabolism: Endogenous and Dietary Routes to Ah Receptor Activation. Drug Metab Dispos 2015, 43:1522–1535.
14. FernandezSalguero PM, Hilbert DM, Rudikoff S, Ward JM, Gonzalez FJ: Aryl-hydrocarbon receptor-deficient mice are resistant to 2,3,7,8-tetrachlorodibenzo-p-dioxin-induced toxicity. Toxicol Appl Pharmacol 1996, 140:173–179.
15. Decad GM, Birnbaum LS, Matthews HB: Distribution and excretion of 2,3,7,8-tetrachlorodibenzofuran in C57BL-6J DBA-2J mice. Toxicol Appl Pharmacol 1981, 59:564–573.
16. Miniero R, De Felip E, Ferri F, di Domenico A: An overview of TCDD half-life in mammals and its correlation to body weight. Chemosphere 2001, 43:839–844.
17. Nichols RG, Zhang JT, Cai JW, Murray IA, Koo I, Smith PB, Perdew GH, Patterson AD: Metatranscriptomic Analysis of the Mouse Gut Microbiome Response to the Persistent Organic Pollutant 2,3,7,8-Tetrachlorodibenzofuran. Metabolites 2020, 10:1.
18. Zhang LM, Hatzakis E, Nichols RG, Hao RX, Correll J, Smith PB, Chiaro CR, Perdew GH, Patterson AD: Metabolomics Reveals that Aryl Hydrocarbon Receptor Activation by Environmental Chemicals Induces Systemic Metabolic Dysfunction in Mice. Environ Sci Technol 2015, 49:8067–8077.
19. Zhang LM, Nichols RG, Correll J, Murray IA, Tanaka N, Smith PB, Hubbard TD, Sebastian A, Albert I, Hatzakis E, et al: Persistent Organic Pollutants Modify Gut Microbiota-Host Metabolic Homeostasis in Mice Through Aryl Hydrocarbon Receptor Activation. Environ Health Perspect 2015, 123:679–688.
20. Yuan PH, Dong MY, Lei HH, Xu GY, Chen G, Song YC, Ma JF, Cheng LM, Zhang LM: Targeted metabolomics reveals that 2,3,7,8-tetrachlorodibenzofuran exposure induces hepatic steatosis in male mice. Environ Pollut 2020, 259:113820.
21. Thursby E, Juge N: Introduction to the human gut microbiota. Biochem J 2017, 474:1823–1836.
22. Singh RK, Chang HW, Yan D, Lee KM, Ucmak D, Wong K, Abrouk M, Farahnik B, Nakamura M, Zhu TH, et al: Influence of diet on the gut microbiome and implications for human health. J Transl Med 2017, 15:73.
23. Zimmermann M, Zimmermann-Kogadeeva M, Wegmann R, Goodman AL: Mapping human microbiome drug metabolism by gut bacteria and their genes. Nature 2019, 570:462–467.
24. Jin YX, Wu SS, Zeng ZY, Fu ZW: Effects of environmental pollutants on gut microbiota. Environ Pollut 2017, 222:1–9.
25. Stark CM, Susi A, Emerick J, Nylund CM: Antibiotic and acid-suppression medications during early childhood are associated with obesity. Gut 2019, 68:62–69.
26. Mbakwa CA, Scheres L, Penders J, Mommers M, Thijs C, Arts ICW: Early Life Antibiotic Exposure and Weight Development in Children. J Pediatr 2016, 176:105–113.
27. Cox LM, Blaser MJ: Antibiotics in early life and obesity. Nat Rev Endocrinol 2015, 11:182–190.

28. Tian Y, Gui W, Rimal B, Koo I, Smith PB, Nichols RG, Cai JW, Liu Q, Patterson AD: Metabolic impact of persistent organic pollutants on gut microbiota. Gut Microbes 2020, 12:1–16.
29. Tian Y, Rimal B, Gui W, Koo I, Yokoyama S, Perdew GH, Patterson AD: Early Life Short-Term Exposure to Polychlorinated Biphenyl 126 in Mice Leads to Metabolic Dysfunction and Microbiota Changes in Adulthood. Int J Mol Sci 2022, 23:8220.
30. Tian Y, Rimal B, Gui W, Koo I, Smith PB, Yokoyama S, Patterson AD: Early Life Polychlorinated Biphenyl 126 Exposure Disrupts Gut Microbiota and Metabolic Homeostasis in Mice Fed with High-Fat Diet in Adulthood. Metabolites 2022, 12:894.
31. Liu Q, Zhang L, Allman EL, Hubbard TD, Murray IA, Hao F, Tian Y, Gui W, Nichols RG, Smith PB, et al: The aryl hydrocarbon receptor activates ceramide biosynthesis in mice contributing to hepatic lipogenesis. Toxicology 2021, 458:152831.
32. Henrick BM, Rodriguez L, Lakshmikanth T, Pou C, Henckel E, Arzoomand A, Olin A, Wang J, Mikes J, Tan ZY, et al: Bifidobacteria-mediated immune system imprinting early in life. Cell 2021, 184:3884–3898.
33. Kim MH, Kang SG, Park JH, Yanagisawa M, Kim CH: Short-Chain Fatty Acids Activate GPR41 and GPR43 on Intestinal Epithelial Cells to Promote Inflammatory Responses in Mice. Gastroenterology 2013, 145:396–406.
34. Husted AS, Trauelsen M, Rudenko O, Hjorth SA, Schwartz TW: GPCR-Mediated Signaling of Metabolites. Cell Metab 2017, 25:777–796.
35. Everard A, Belzer C, Geurts L, Ouwerkerk JP, Druart C, Bindels LB, Guiot Y, Derrien M, Muccioli GG, Delzenne NM, et al: Cross-talk between Akkermansia muciniphila and intestinal epithelium controls diet-induced obesity. Proc Natl Acad Sci U S A 2013, 110:9066–9071.
36. Yoon HS, Cho CH, Yun MS, Jang SJ, You HJ, Kim JH, Han D, Cha KH, Moon SH, Lee K, et al: Akkermansia muciniphila secretes a glucagon-like peptide-1-inducing protein that improves glucose homeostasis and ameliorates metabolic disease in mice. Nat Microbiol 2021, 6:563–573.
37. Depommier C, Everard A, Druart C, Plovier H, Van Hul M, Vieira-Silva S, Falony G, Raes J, Maiter D, Delzenne NM, et al: Supplementation with Akkermansia muciniphila in overweight and obese human volunteers: a proof-of-concept exploratory study. Nat Med 2019, 25:1096–1103.
38. Dekoning EP, Karmaus W: PCB exposure in utero and via breast milk. A review. J Expo Anal Environ Epidemiol 2000, 10:285–293.
39. Tai PT, Nishijo M, Kido T, Nakagawa H, Maruzeni S, Naganuma R, Nguyen TNA, Morikawa Y, Luong HV, Anh TH, et al: Dioxin Concentrations in Breast Milk of Vietnamese Nursing Mothers: A Survey Four Decades after the Herbicide Spraying. Environ Sci Technol 2011, 45:6625–6632.
40. Pohl HR, Hibbs BF: Breast-feeding exposure of infants to environmental contaminants - A public health risk assessment viewpoint: Chlorinated dibenzodioxins and chlorinated dibenzofurans. Toxicol Ind Health 1996, 12:593–611.
41. van den Berg M, Kypke K, Kotz A, Tritscher A, Lee SY, Magulova K, Fiedler H, Malisch R: WHO/UNEP global surveys of PCDDs, PCDFs, PCBs and DDTs in human milk and benefit-risk evaluation of

breastfeeding. Arch Toxicol 2017, 91:83–96.

42. Selevan SG, Kimmel CA, Mendola P: Identifying critical windows of exposure for children's health. Environ Health Perspect 2000, 108:451–455.
43. Arrieta MC, Stiemsma LT, Amenyogbe N, Brown EM, Finlay B: The intestinal microbiome in early life: health and disease. Front Immunol 2014, 5:427.
44. Gensollen T, Iyer SS, Kasper DL, Blumberg RS: How colonization by microbiota in early life shapes the immune system. Science 2016, 352:539–544.
45. Shao XQ, Ding XL, Wang B, Li L, An XF, Yao QM, Song RH, Zhang JA: Antibiotic Exposure in Early Life increases Risk of Childhood Obesity: A Systematic Review and Meta-Analysis. Front Endocrinol 2017, 8:170.
46. Guo WL, Mao BY, Cui SM, Tang X, Zhang QX, Zhao JX, Zhang H: Protective Effects of a Novel Probiotic Bifidobacterium pseudolongum on the Intestinal Barrier of Colitis Mice via Modulating the Ppar gamma/STAT3 Pathway and Intestinal Microbiota. Foods 2022, 11.
47. Boulange CL, Neves AL, Chilloux J, Nicholson JK, Dumas ME: Impact of the gut microbiota on inflammation, obesity, and metabolic disease. Genome Med 2016, 8:42.
48. Gerard P: Gut microbiota and obesity. Cell Mol Life Sci 2016, 73:147–162.
49. Tolhurst G, Heffron H, Lam YS, Parker HE, Habib AM, Diakogiannaki E, Cameron J, Grosse J, Reimann F, Gribble FM: Short-Chain Fatty Acids Stimulate Glucagon-Like Peptide-1 Secretion via the G-Protein-Coupled Receptor FFAR2. Diabetes 2012, 61:364–371.
50. Kaji L, Karaki S, Kuwahara A: Short-Chain Fatty Acid Receptor and Its Contribution to Glucagon-Like Peptide-1 Release. Digestion 2014, 89:31–36.
51. Zarrinpar A, Chaix A, Xu ZJZ, Chang MW, Marotz CA, Saghatelian A, Knight R, Panda S: Antibiotic-induced microbiome depletion alters metabolic homeostasis by affecting gut signaling and colonic metabolism. Nat Commun 2018, 9:2872.
52. Wren AM, Bloom SR: Gut hormones and appetite control. Gastroenterology 2007, 132:2116–2130.
53. Dao MC, Everard A, Aron-Wisnewsky J, Sokolovska N, Prifti E, Verger EO, Kayser BD, Levenez F, Chilloux J, Hoyles L, et al: Akkermansia muciniphila and improved metabolic health during a dietary intervention in obesity: relationship with gut microbiome richness and ecology. Gut 2016, 65:426–436.
54. Meng D, Sommella E, Salviati E, Campiglia P, Ganguli K, Djebali K, Zhu WS, Walker WA: Indole-3-lactic acid, a metabolite of tryptophan, secreted by Bifidobacterium longum subspecies infantis is anti-inflammatory in the immature intestine. Pediatr Res 2020, 88:209–217.
55. Tian Y, Gui W, Koo I, Smith PB, Allman EL, Nichols RG, Rimal B, Cai JW, Liu Q, Patterson AD: The microbiome modulating activity of bile acids. Gut Microbes 2020, 11:979–996.
56. Virtue S, Vidal-Puig A: GTTs and ITTs in mice: simple tests, complex answers. Nat Metab 2021, 3:883–886.

57. Shi XH, Xiao CN, Wang YL, Tang HR: Gallic Acid Intake Induces Alterations to Systems Metabolism in Rats. J Proteome Res 2013, 12:991–1006.
58. Amiel A, Tremblay-Franco M, Gautier R, Ducheix S, Montagner A, Polizzi A, Debrauwer L, Guillou H, Bertrand-Michel J, Canlet C: Proton NMR Enables the Absolute Quantification of Aqueous Metabolites and Lipid Classes in Unique Mouse Liver Samples. Metabolites 2020, 10:9.
59. Tian Y, Nichols RG, Cai JW, Patterson AD, Cantorna MT: Vitamin A deficiency in mice alters host and gut microbial metabolism leading to altered energy homeostasis. J Nutr Biochem 2018, 54:28–34.
60. Dong FC, Hao FH, Murray IA, Smith PB, Koo I, Tindall AM, Kris-Etherton PM, Gowda K, Amin SG, Patterson AD, Perdew GH: Intestinal microbiota-derived tryptophan metabolites are predictive of Ah receptor activity. Gut Microbes 2020, 12:1–24.
61. Tsugawa H, Cajka T, Kind T, Ma Y, Higgins B, Ikeda K, Kanazawa M, VanderGheynst J, Fiehn O, Arita M: MS-DIAL: data-independent MS/MS deconvolution for comprehensive metabolome analysis. Nat Methods 2015, 12:523–526.
62. Barupal DK, Haldiya PK, Wohlgemuth G, Kind T, Kothari SL, Pinkerton KE, Fiehn O: MetaMapp: mapping and visualizing metabolomic data by integrating information from biochemical pathways and chemical and mass spectral similarity. BMC Bioinform 2012, 13:99.
63. Tian Y, Nie X, Xu S, Li Y, Huang T, Tang HR, Wang YL: Integrative metabonomics as potential method for diagnosis of thyroid malignancy. Sci Rep 2015, 5:14869.
64. An YP, Xu WX, Li HH, Lei HH, Zhang LM, Hao FH, Duan YX, Yan X, Zhao Y, Wu JF, et al: High-Fat Diet Induces Dynamic Metabolic Alterations in Multiple Biological Matrices of Rats. J Proteome Res 2013, 12:3755–3768.
65. Cai JW, Nichols RG, Koo I, Kalikow ZA, Zhang LM, Tian Y, Zhang JT, Smith PB, Patterson AD: Multiplatform Physiologic and Metabolic Phenotyping Reveals Microbial Toxicity. Msystems 2018, 3:e00123-00118.
66. Chen SF, Zhou YQ, Chen YR, Gu J: fastp: an ultra-fast all-in-one FASTQ preprocessor. Bioinformatics 2018, 34:884–890.
67. Blanco-Miguez A, Beghini F, Cumbo F, McIver LJ, Thompson KN, Zolfo M, Manghi P, Dubois L, Huang KD, Thomas AM, et al: Extending and improving metagenomic taxonomic profiling with uncharacterized species using MetaPhlAn 4. Nat Biotechnol 2023.
68. Hu YJ, Satten GA: Testing hypotheses about the microbiome using the linear decomposition model (LDM). Bioinformatics 2020, 36:4106–4115.
69. Beghini F, McIver LJ, Blanco-Miguez A, Dubois L, Asnicar F, Maharjan S, Mailyan A, Manghi P, Scholz M, Thomas AM, et al: Integrating taxonomic, functional, and strain-level profiling of diverse microbial communities with bioBakery 3. Elife 2021, 10.
70. Wood DE, Lu J, Langmead B: Improved metagenomic analysis with Kraken 2. Genome Biol 2019, 20:257.
71. Langmead B, Salzberg SL: Fast gapped-read alignment with Bowtie 2. Nat Methods 2012, 9:357–359.

72. Okonechnikov K, Conesa A, Garcia-Alcalde F: Qualimap 2: advanced multi-sample quality control for high-throughput sequencing data. Bioinformatics 2016, 32:292–294.
73. Liao Y, Smyth GK, Shi W: The R package Rsubread is easier, faster, cheaper and better for alignment and quantification of RNA sequencing reads. Nucleic Acids Res 2019, 47:e47.
74. Love MI, Huber W, Anders S: Moderated estimation of fold change and dispersion for RNA-seq data with DESeq2. Genome Biol 2014, 15:550.
75. Koblitz J, Schomburg D, Neumann-Schaal M: MetaboMAPS: Pathway sharing and multi-omics data visualization in metabolic context. F1000Res 2020, 9:288.

Figures

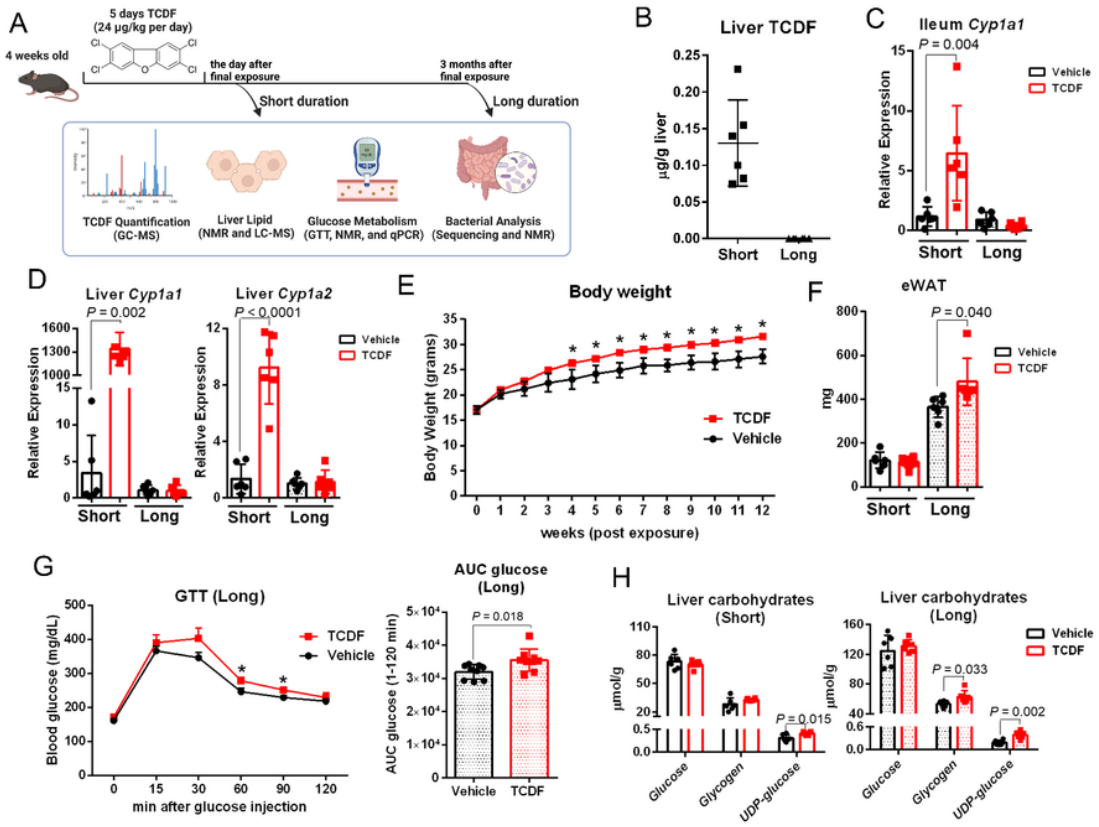

Fig. 1

Figure 1

Early-life TCDF exposure leads to persistent weight gain and glucose intolerance after TCDF is eliminated from the body. (**A**) Experimental schematic for determining the short and long duration effect of early life TCDF exposure. (**B**) TCDF levels in the liver of mice at three months after exposure were below the limit of detection via quantitative GC-MS analysis (n = 6). (**C-D**) qPCR analysis showed dramatically increased levels of AHR targeted genes in the ileum and liver after five days exposure but unchanged three months after exposure (n = 6). (**E-F**) Five days of TCDF exposure significantly increased body weight and epididymal white adipose tissue (eWAT) weight later in life (n = 6). $P = 0.9848$ W0, $P = 0.0460$ W6, $P = 0.0339$ W7, $P = 0.0201$ W8, $P = 0.0327$ W9, $P = 0.0470$ W10, $P = 0.0389$ W11, $P = 0.0203$ W12. (**G**) Blood

glucose levels following intraperitoneal injection of glucose and the area under the curve (AUC) indicated impaired glucose tolerance with TCDF exposure later in life (n = 9). *P* = 0.0465 60_min, *P* = 0.0212 90_min. (**H**) Targeted ^{1}H NMR analysis indicated significantly higher levels of liver glycogen and UDP-glucose with TCDF exposure later in life (n = 6). All *P* values were calculated using two-tailed unpaired t test or Mann-Whitney U test. All graphs are presented as Mean ± SD.

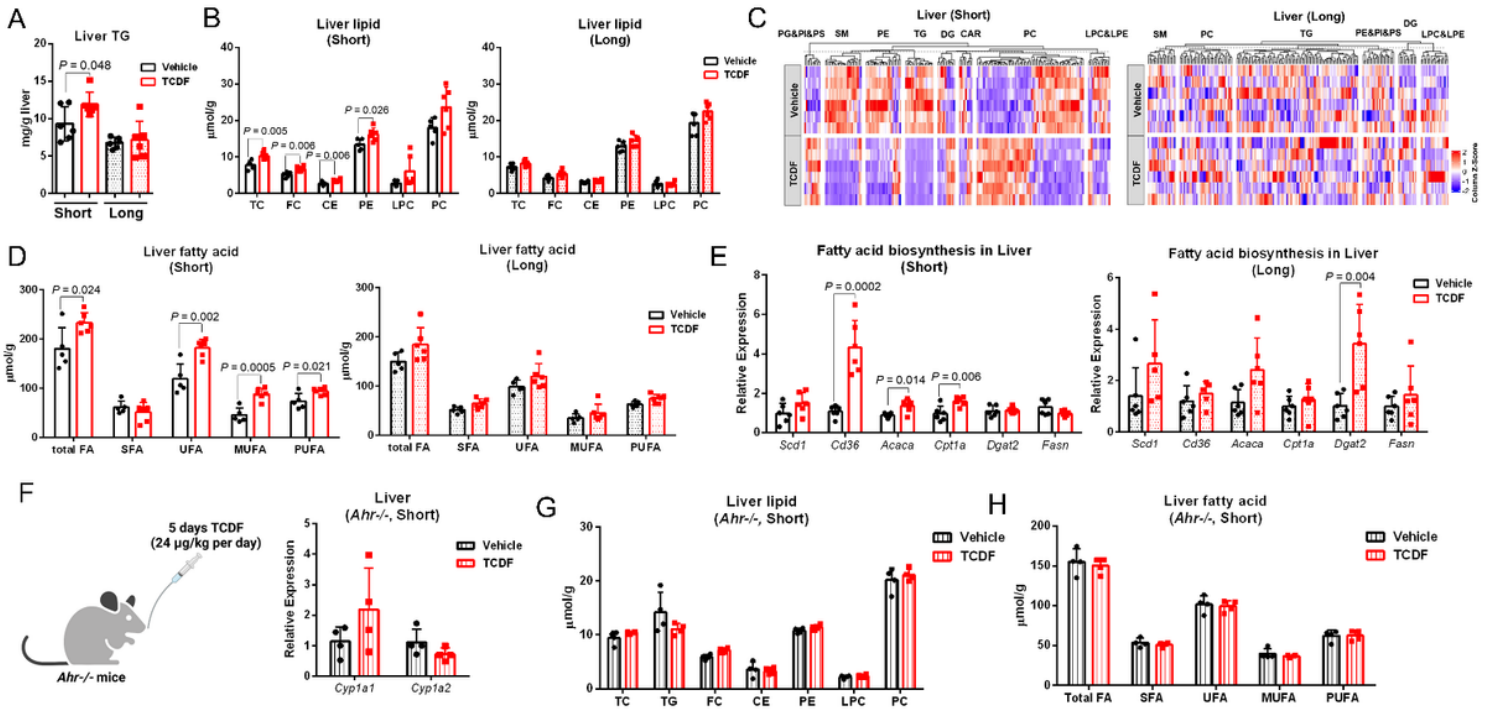

Fig. 2

Figure 2

Early-life TCDF exposure increases liver lipogenesis in an AHR-dependent manner. (**A**) TCDF exposure rapidly increased liver triglyceride (TG) levels in the mice (n = 6). (**B-C**) Quantitative ^{1}H NMR and global UHPLC-MS/MS analysis of liver lipid profiling revealed TCDF exposure rapidly increased liver lipogenesis (n = 6). Red shades represent metabolites that are increased, and blue shades represent metabolites that are decreased in heatmap. *P* values were presented in Supplementary Table S2. (**D-E**) Quantitative ^{1}H NMR and qPCR analysis indicated that TCDF rapidly increased liver *de novo* fatty acid biosynthesis (n = 6). (**F**) qPCR analysis revealed no AHR activation in liver from *Ahr-/-* mice after five days of TCDF exposure (n = 4). (**G-H**) Quantitative ^{1}H NMR analysis of liver lipids and fatty acids showed no changes in lipid profile in *Ahr-/-* mice after five days of TCDF exposure (n = 4). TC, total cholesterol; FC, free cholesterol; CE, cholesterol ester; PE, phosphatidylethanolamine; LPC, lysophosphatidylcholine; PC, phosphatidylcholine; PG, phosphatidylglycerol; PS, phosphatidylserine; SM, sphingomyelin; DG, diglycerol; CAR, carnitine; LPE, lysophosphatidylethanolamine; PI, phosphoinositide; FA, fatty acid; SFA, saturated fatty acid; UFA, unsaturated fatty acid; MUFA, monosaturated fatty acid; PUFA, polyunsaturated fatty acid.

P values were calculated using two-tailed unpaired t test or Mann-Whitney U test. All graphs are presented as Mean ± SD.

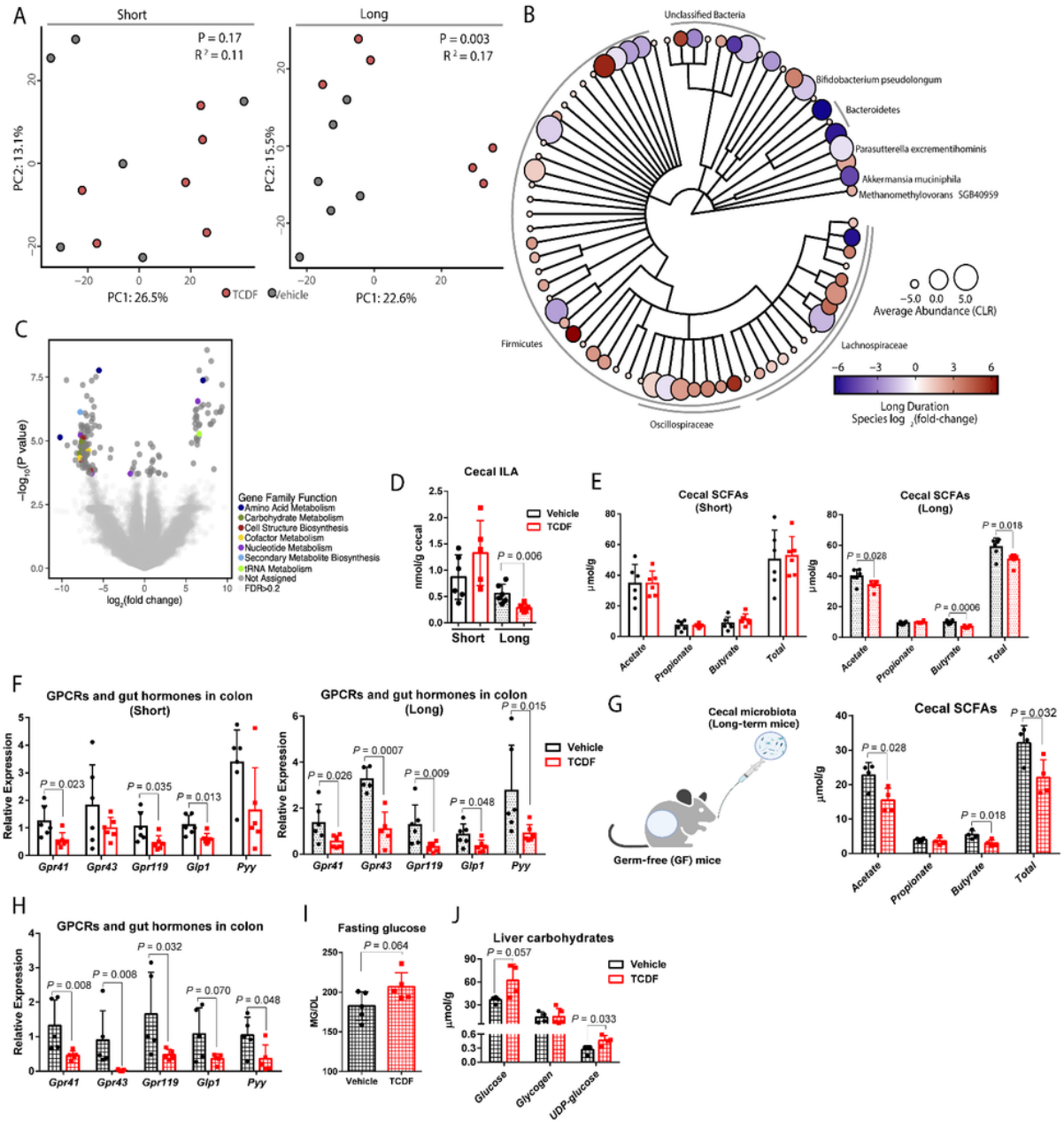

Figure 3

Early-life TCDF impacts the gut microbiome composition and function later in life. (**A**) Analysis of cecal species-level abundances reveals significant effects of TCDF exposure on microbiome composition only later in life (n = 6, principal coordinates analysis of CLR Euclidean distances with statistical testing by PERMANOVA). (**B**) Phylogenetically diverse taxa are impacted later in life including *A. muciniphila* (FDR < 0.2, cladogram shown depicts taxonomic hierarchy of statistically significant species, Supplementary Table S3). (**C**) Analysis of differentially abundant gene families uncovers amino acid, nucleotide, and carbohydrate metabolism (FDR < 0.2, Supplementary Table S4). (**D**) Quantitative UHPLC-MS analysis

showed significant lower level of tryptophan metabolite indole-3-lactic acid (ILA) with TCDF exposure later in life (n = 6). (**E**) Targeted ^{1}H NMR analysis showed significant lower levels of cecal short chain fatty acids (SCFAs) levels with TCDF exposure later in life (n = 6). (**F**) qPCR analysis showed significant lower levels of gene expression levels of *Gpr41*, *Gpr43*, *Gpr119*, *Glp1*, and *Pyy* in the colon with TCDF exposure later in life (n = 6). (**G**) Targeted ^{1}H NMR analysis indicated GF recipients from TCDF exposed mice exhibited significantly lower levels of cecal SCFAs (n = 4). (**H**) qPCR analysis revealed GF recipients from TCDF exposed mice exhibited significantly lower gene expression levels of *Gpr41*, *Gpr43*, *Gpr119*, and *Pyy* in the colon (n = 5). (**I**) GF recipients from TCDF exposed mice showed mildly higher fasting glucose levels (n = 5). (**J**) Targeted ^{1}H NMR analysis showed significant higher levels of liver UDP-glucose in GF recipients from TCDF exposed mice (n = 4). *P* values were calculated using two-tailed unpaired t test or Mann-Whitney U test. All graphs are presented as Mean ± SD.

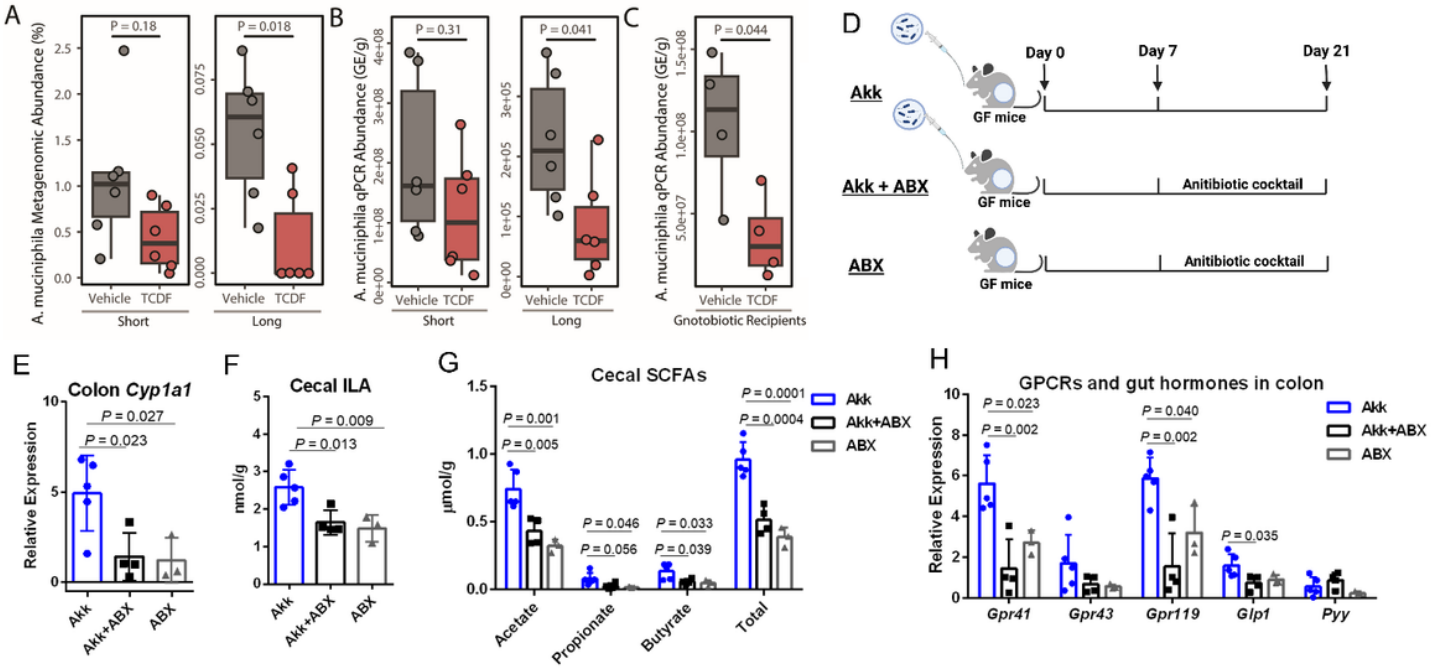

Fig. 4

Figure 4

A. muciniphila is negatively correlated with TCDF exposure and its administration promotes production of ILA and SCFAs

(**A-B**) Metagenomics and qPCR analysis revealed that TCDF exposure resulted in significantly lower abundances of cecal *A. muciniphila* later in life (n = 6). (**C**) qPCR analysis indicated that GF recipients from TCDF exposed mice exhibited significantly lower abundances of cecal *A. muciniphila* (n = 4). (**D**) Experimental schematic for determining the functional role of *A. muciniphila* that is negatively correlated with TCDF exposure in vivo. GF mice with antibiotic treatment (ABX) are used as controls. (**E**) qPCR

analysis revealed significantly higher gene expression levels of *Cyp1a1* in the colon from GF mice colonized with *A. muciniphila* (n = 3-5). (**F**) *A. muciniphila* administration promotes production of cecal indole-3-lactic acid (ILA) in GF mice using UHPLC-MS analysis (n = 3-5). (**G**) *A. muciniphila* administration promotes production of cecal short chain fatty acids (SCFAs) in GF mice using targeted ^{1}H NMR analysis (n = 3-5). (**H**) *A. muciniphila* administration significantly increased gene expression levels of *Gpr41*, *Gpr119*, and *Glp1* in the colon from GF mice using qPCR analysis (n = 3-5). *P* values were calculated using one-way ANOVA test with Dunnett's multiple comparisons. All graphs are presented as Mean ± SD or median and interquartile ranges.

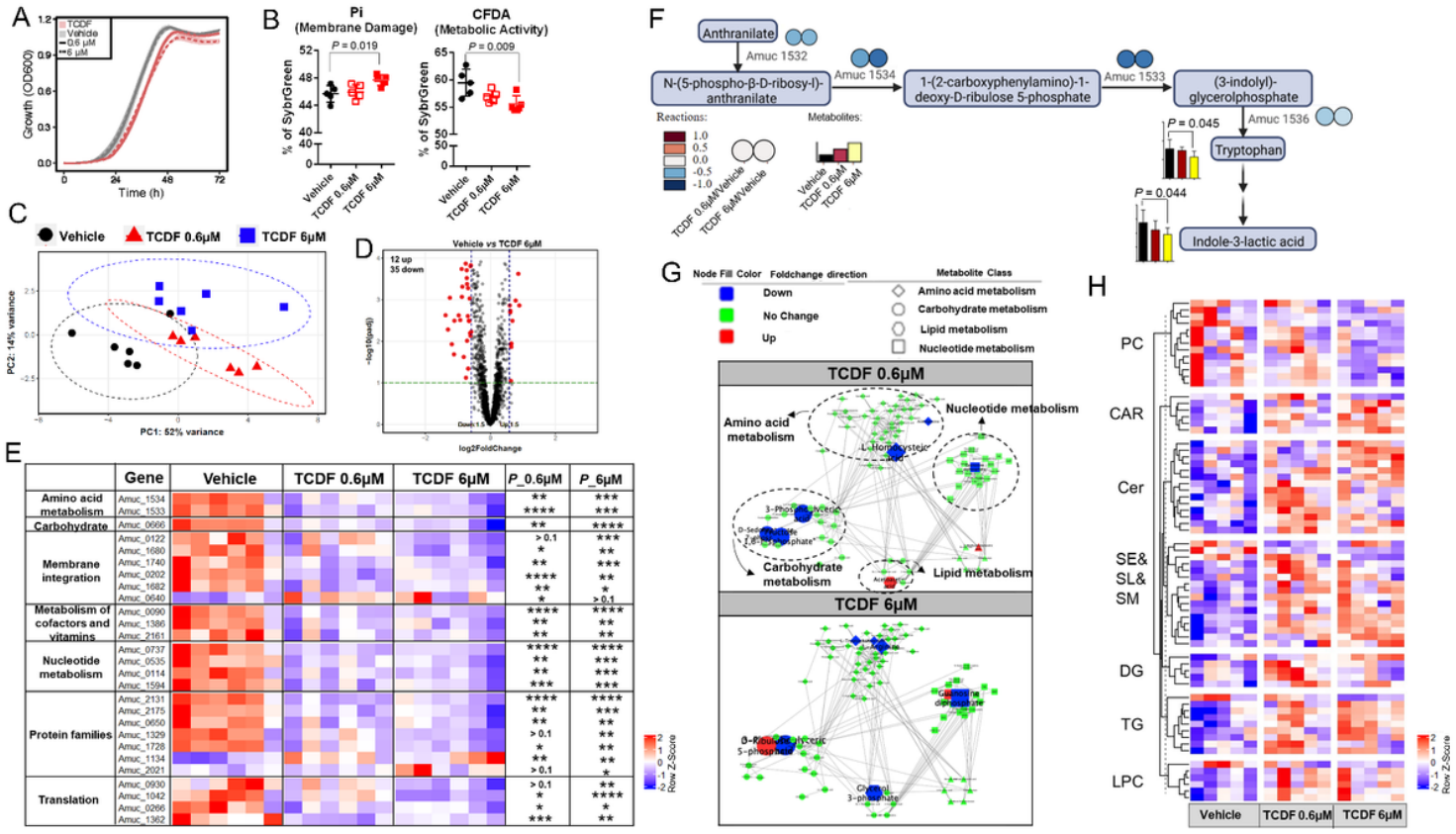

Figure 5

TCDF exposure significantly affects the metabolism of *A. muciniphila* in vitro. (**A**) Two doses of TCDF exposure slowed the growth rate of *A. muciniphila* as measured by absorbance (OD 600) over 72 hours (n = 3). (**B**) *A. muciniphila* with TCDF exposure (6 µM) exhibited increased damaged bacteria (Pi-stained) and lower metabolic activity (CFDA-stained) using flow cytometric analyses after 36 h incubation (n = 5). (**C-D**) The transcriptome of *A. muciniphila* is significantly impacted by TCDF exposure as demonstrated by PCA analysis (C) and a volcano plot of differentially expressed genes (D) after 36 h incubation (n = 6). (**E**) Gene orthologs involved in amino acid, carbohydrate, nucleotide metabolism, membrane integration, vitamin metabolism, and translation pathways were most significantly reduced in *A. muciniphila* with TCDF exposure after 36 h incubation (n = 6). Red shades represent gene orthologs that are increased, and blue shades represent gene orthologs that are decreased. * $P < 0.1$, ** $P < 0.01$, *** $P < 0.001$, **** $P < 0.0001$, *P* values were presented in Supplementary Table S7. (**F**) TCDF exposure (6 µM) significantly

downregulated *A. muciniphila*-derived indole-3-lactic acid pathway after 36 h incubation visualizing by transcriptomics data combined with metabolomics data (n = 6). (**H-I**) TCDF exposure resulted in significant changes in global metabolism including lipid metabolism in *A. muciniphila* after 36 h incubation using UHPLC-MS-based metabolomics analysis (n = 6). Red shades represent metabolites that are increased, and blue shades represent metabolites that are decreased. PC, phosphatidylcholine; CAR, carnitine; Cer, ceramide; SL, sphingolipid; SM, sphingomyelin; DG, diglycerol; TG, triglyceride; LPC, lysophosphatidylcholine. (B) and (G-H) *P* values were calculated using one-way ANOVA test with Dunnett's multiple comparisons. (D-F) Adjusted *P* values were calculated using Tukey's correction. All graphs are presented as Mean ± SD.

Supplementary Files

This is a list of supplementary files associated with this preprint. Click to download.

- TCDFearlylifesu.docx
- TableS2.xlsx
- TableS3.xlsx
- TableS4.xlsx
- TableS7.xlsx
- TableS9.xlsx
- TableS10.xlsx